Development of Machine Learning-Assisted Spectra Analyzer for the NEWCUT Muon Spectrometer

László Oláh,[1,2] Hiroyuki K. M. Tanaka,[1,2] Hiroshi Suenaga,[1,3] Shinichi Miyamoto,[1,4] Gábor Galgóczi,[1,5] Gergő Hamar,[1,5] and Dezső Varga[1,5]

[1]*International Virtual Muography Institute (Global)*

[2]*Earthquake Research Institute, The University of Tokyo, Tokyo 113-0032, Japan*

[3]*Central Research Institute of Electric Power Industry (CRIEPI), Chiba 270-1194, Japan*

[4]*NEC Corporation (Global)*

[5]*Wigner Research Centre for Physics, Eötvös Loránd Research Network, Budapest 1121, Hungary*

Corresponding author: László Oláh
Email: olah.laszlo@wigner.hu

Abstract

The precise measurement of low-energy muon spectra is required to improve muography of small-sized objects. The NEWCUT spectrometer is a 6-meter-length, rotatable, Multiwire-Proportional-Chamber-based spectrometer that is developed for the measurement of the low-energy spectra of cosmic-ray muons up to a few GeV between vertical and horizontal directions. The spectrometer consists of a consecutive series of nineteen detectors with a positional resolution of approx. 3.5 mm each and lead plates. A neural network-assisted muon spectra analyzer was implemented and trained using GEANT4 simulated data. The energy-dependent relative differences between the simulated and reconstructed muons suggest that the actual experimental arrangement can accurately measure the spectra up to an energy of 6 GeV.

Keywords: muography, muon spectra, tracking detector, Monte Carlo simulation, GEANT4, machine learning, neural network
DOI: 10.31526/JAIS.2022.264

1. INTRODUCTION

Cosmic-ray muons are elementary charged particles created continuously as decay products of hadronic cascades originating from the collisions of isotropically arriving galactic cosmic particles with the atmospheric nuclei [1]. The zenith-angle and energy-dependent muon fluxes, called muon spectra, were measured in the atmosphere, on the Earth's surface and under various overburden materials; see various compiled data sets in [2, 3]. Muon spectra measurements were applied for revealing and investigating various physical and geophysical phenomena: the high-energy (beyond a few tens of GeV) muon spectrum probes the cosmic particle generation even beyond the energies of particle accelerator-based experiments [4, 5], improves the understanding of the evolution of extensive air showers [4, 6], helps to estimate the atmospheric neutrino fluxes [7], tests the neutrino oscillation mechanism [8], etc. The low-energy regime (up to a few GeV) of the muon spectrum can be utilized for the investigation of the effect of Earth's magnetic field [9] and physical properties of the atmosphere [10] on their propagation, estimating the cosmogenic nuclei created in the atmosphere and in rocks [9], studying neutrino decays [11, 12, 13, 14], etc.

Muography is an imaging technique that quantifies the amount of materials in various human-made and natural structures by the measurement of the angular-dependent flux of penetrating muons; see, e.g., [15, 16, 17], similarly to X-ray radiography of the human body. The imaging process of muography is fed with the muon spectra to simulate or calculate the flux of penetrated muons. The accurate muographic imaging of small-scale (up to a few tens of meters thick) objects requires the extension and improvement of angular-dependent muon spectra data sets at low energies. Furthermore, accurate momentum measurement is expected to improve various applications of muon imaging from material identification by means of the measurement of muons' multiple scattering [18] to low-noise muography of volcanoes [19].

Different techniques have been utilized for the measurement and discrimination of muons' momentum. These techniques are based on the measurement of muons' time-of-flight [20], detection of Cherenkov radiation emitted by muons in dielectric media [21, 22], reconstruction of the bending of muons' trajectory in magnetic field [5], multiple scattering and absorption of muons [8, 23, 24], etc.

An international collaboration with the participation of **NE**C Corporation, **W**igner RCP, **C**RIEPI, and The **U**niversity of **T**okyo, shortly NEWCUT, constructed a rotatable muon spectrometer to quantify the low-energy muon spectra by means of precise measurement of absorption and multiple scattering of incident muons. The analysis framework of NEWCUT is under development. This work focuses on a machine-learning-based muon spectra analyzer. This paper is organized as follows. We present the instrument in Section 2, the simulation method in Section 3 and the machine-learning-based energy classification method in Section 4.

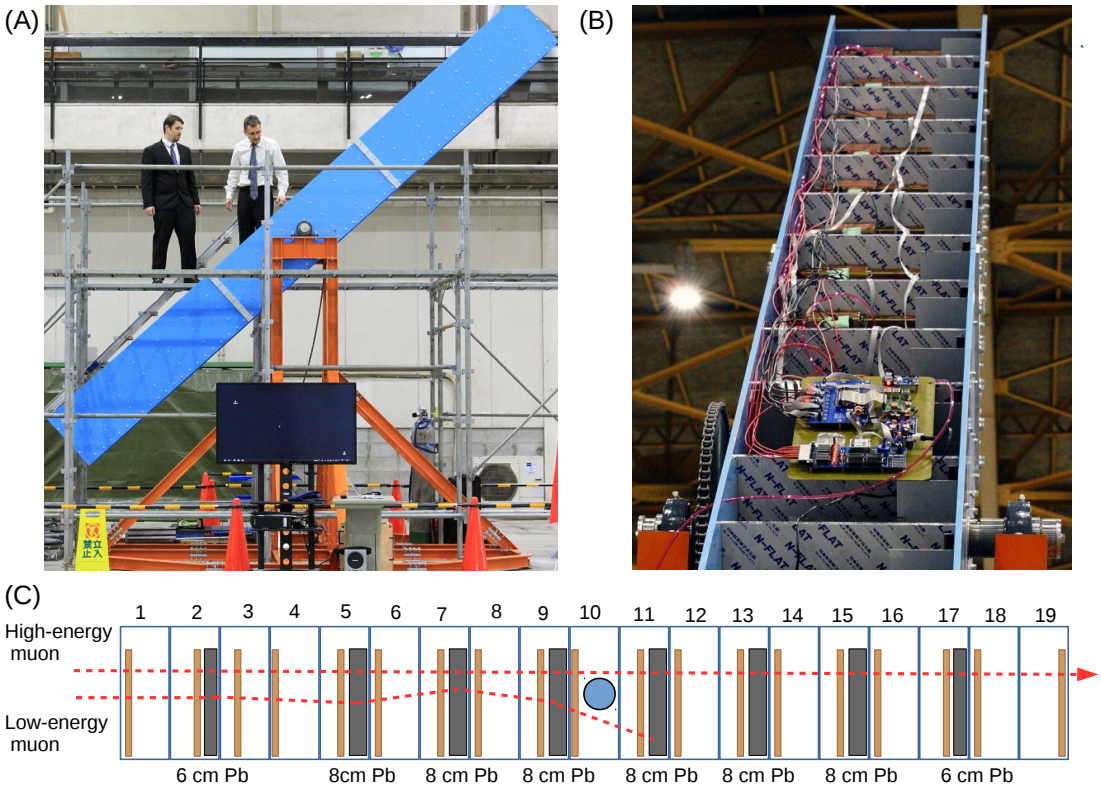

FIGURE 1: The NEWCUT spectrometer. (A) Photograph from a side view. (B) Photograph from a front view. (C) The schematic drawing of the experimental arrangement from a side view. The brown and gray rectangles represent the detectors and lead plates, respectively. The blue circle shows the rotation axis of the spectrometer. The red dashed lines show typical trajectories of low-energy and high-energy muons in the spectrometer.

2. THE MULTIWIRE-PROPORTIONAL-CHAMBER-BASED MUON SPECTROMETER

Our muon spectrometer is under development at the research facility of NEWCUT in Chiba, Japan, at the latitude of N 35.877° and longitude of E 140.028° at 20 m above sea level. The instrument is housed in a 6-meter-length rotatable iron support structure that allows measuring the angular dependent muon spectra between vertical and horizontal directions. The tracking system consists of a consecutive series of nineteen 40 cm $\times$ 40 cm sized Multiwire Proportional Chambers (MWPC) [25]. Each MWPC is segmented with two perpendicular wire planes with segmentation of 12 mm [26]. This detector design provides a position resolution of approx. 3.5 mm. Besides MWPCs, lead plates are installed between the MWPCs with the variable number and variable thickness to deflect and absorb the incident particles. Each lead plate has a height of 40 cm and a width of 20 cm. Currently, eight layers of lead plates are used between the MWPCs with a total thickness of 60 cm. Each lead layer is aligned to the middle of MWPCs in the horizontal dimension. The tracking system is divided into 19 racks by 1-cm-thick Al plates for fixing the positions of MWPCs and lead plates. Figure 1 shows two photographs of the tracking system from front (A) and side (B) views, as well as the schematic drawing of the actual experimental arrangement (C).

An environmentally friendly Ar-CO_2 gas mixture (Ar:80%, CO_2:20%) flows continuously across the tracking system with a moderated flow rate of approx. 1 liter per hour. The signal production is initiated by means of ionization of gas atoms by the penetrated charged particles. A high voltage of +1,750 V is applied to the anode wires to provide a measurable signal of a few thousand electrons. The signals are read out by custom-designed electronics [26]. The data acquisition and detector control are managed by a microcomputer. The data readout is triggered by the coincidence of at least three MWPCs. Each detector layer operates with a triggering efficiency of approx. 99%. The trigger is blocked for a few hundreds of microseconds during the data readout. The data files are written event-by-event with the track positions on each MWPC, the trigger pattern with its timing, and the analog signal amplitudes (ADC) as ASCII files. An extensive description of the construction of MWPCs and their readout system are described in Varga et al. [27].

3. GEANT4 SIMULATION OF THE NEWCUT SPECTROMETER

The training of the machine learning model was performed with Monte Carlo simulation data. The structure of NEWCUT spectrometer and the penetration of muons through the tracking system were simulated in the GEANT4 framework [28].

500,000 muons were generated and injected into the detector structure from a $50 \times 50\,\mathrm{cm}^2$-sized flat surface by the EcoMug generator [29]. The standard physics list with all the relevant electromagnetic processes was applied to accurately simulate the interaction of particles with the transversed materials. The positional coordinates and energy deposits of muons in the Ar gas were recorded for each tracking layer. The simulated positional coordinates were shifted with random distances that followed zero-centered Gaussian distributions with sigma values that were equal to the position resolutions of MWPCs.

The energy deposits are related to the measured analog signal amplitudes. These simulated quantities were used to adjust the detection efficiencies on a MWPC-by-MWPC basis. Figure 2(A) shows an example of the energy threshold dependency of detection efficiency. The thresholds were set to 1.75 eV to achieve the detection efficiency of approx. 98% for each MWPC. For accurate modeling of experimental data, the frequency distributions of simulated energy deposit values, dE, were adjusted to the frequency distributions of the measured ADC values by $p_0 + p_1 \times dE$ functions on chamber-by-chamber, where p_0 and p_1 were different parameters for the different chambers. Figure 2(B) shows the histograms of scaled simulated energy deposit distribution (black) and experimental analog signal amplitude distribution (red). Although a slight difference is observed between the simulation and experimental data histograms because the simulation does not accurately model the flux muon of high-energy (beyond a few tens of GeVs), it does not affect this work because we are focusing on the low-energy spectra.

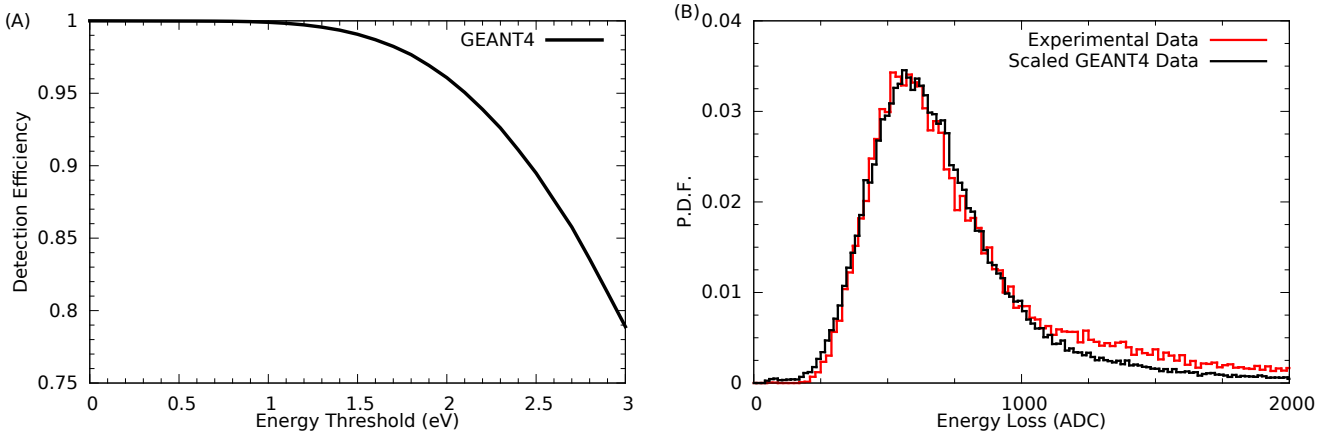

FIGURE 2: (A) The detection efficiency of muons is shown as a function of the energy threshold for Ar gas. The simulated energy loss distributions (black histogram) were scaled to the measured analog signal amplitudes (red histogram) on chamber-by-chamber basis. Panel (B) shows an example for the first detector layer.

4. A NEURAL-NETWORK-BASED MUON SPECTRUM ANALYZER

4.1. *Construction and Training of Neural Network*

Machine learning [30] is an applicable technique for quantification of the muon spectra by means of classification of the energy of detected particles on a track-by-track basis. In this work, we applied a model that combines four neural networks. The simulated data set was divided into three subsets in a proportion of 0.6 : 0.2 : 0.2 for training, validating, and testing of the model. The neural networks were implemented, trained, and tested with scikit-learn version 0.22.1 [31], Keras version 2.4.3 [32], and Tensorflow version 2.3.0 [33].

The structure of the implemented model is shown in Figure 3. The input of the model was fed with 19 horizontal coordinates, 19 vertical coordinates, and 19 ADC (adjusted energy deposit) values. The three different data sets were learned by three independent neural networks. The outputs of these neural networks were concatenated into a fourth neural network. The neurons of input and hidden layers were activated by Rectified Linear Unit (ReLU) functions. The output of the fourth neural network was a classifier layer, where the neurons were activated by Softmax functions. Each output neuron corresponded to an energy bin and the output values provided the energy probabilities. The size of energy bins was chosen to be 0.25 GeV. 40 neurons were applied at the output of the neural network; thus all muons with energies of above 10 GeV were classified into the last energy bin.

The weights of neurons were optimized with the Adam method which is a gradient-based optimization algorithm [34]. Bayesian optimization was utilized for hyperparameter tuning of the neural networks with 100 epochs. The relative difference between the generated and predicted spectra, $(N_{\mathrm{predicted}} - N_{\mathrm{generated}})/N_{\mathrm{generated}}$, was calculated to determine the optimal hyperparameters. The optimal number of hidden layers was found to be 3 for each neural network. The optimal number of neurons was found to be 512 for each hidden layer. The learning rate and the exponential decay rate parameters of the Adam method were found to be 0.0001 and 0.99, respectively.

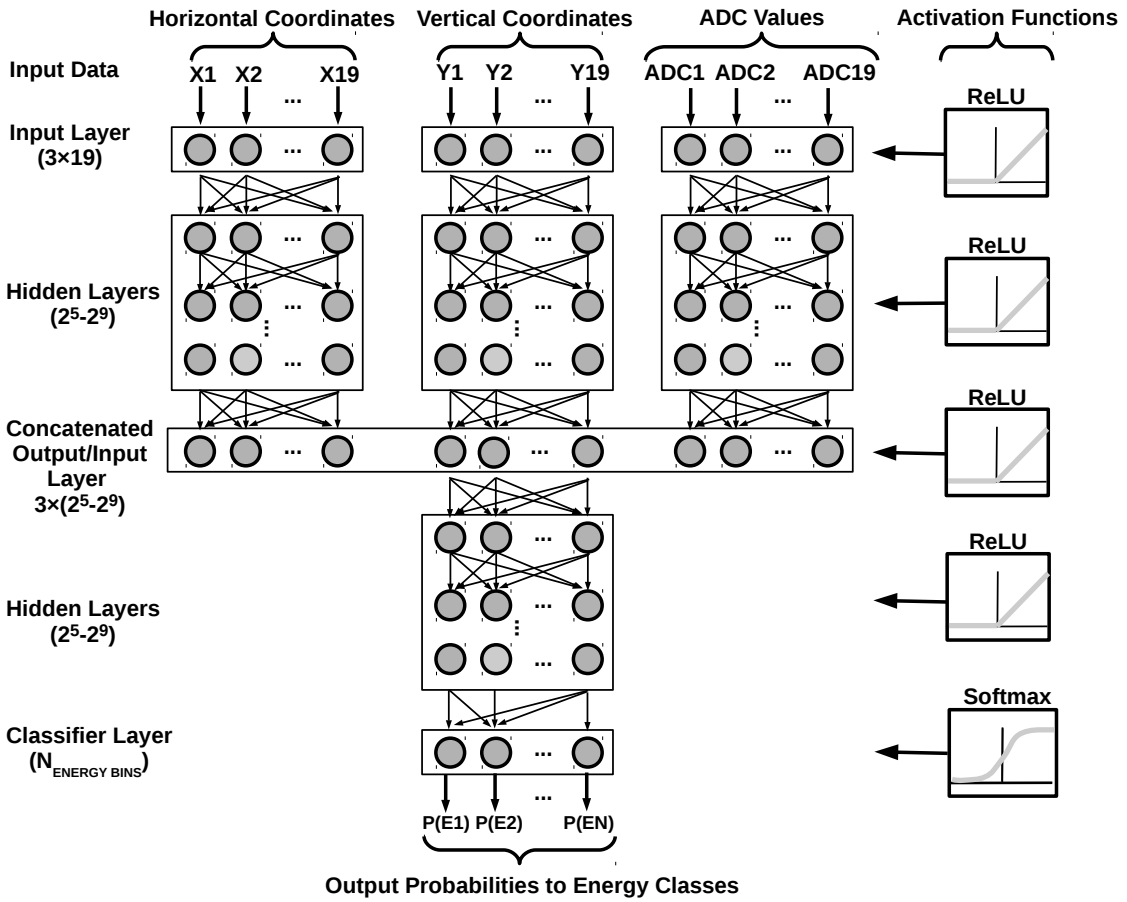

FIGURE 3: Schematic drawing of the neural-network-based model that was applied for track-by-track energy classification.

4.2. Preliminary Results

Figure 4(A) shows the normalized number of muons as a function of predicted energy and simulated energy. The number of muons was normalized with the mode values of the frequency distributions of predicted energies in each bin. Figure 4(B) shows the average predicted energies with 1 standard deviation error bars that were extracted for the vertical slices of Figure 4(A). The average predicted energies were found slightly above the generated energies. The predicted energies show a fair correlation with the generated energies up to 6 GeV.

The predicted energies saturate at 6 GeV for the NEWCUT spectrometer. This effect is assumed to be the existence of an energy (momentum) threshold above which the spatial displacements due to muons' multiple scattering are smeared by the positional resolution of the tracking detector. Figure 5 shows predicted energies as a function of generated energies for our experimental apparatus with three different position resolutions: $1\sigma_{\mathrm{pos}}$ (black circles, the same as shown in Figure 4(B)), $2\sigma_{\mathrm{pos}}$ (blue rectangles), and $4\sigma_{\mathrm{pos}}$ (red triangles), respectively. The predicted energies are slightly increased relatively to the generated energies and saturated at smaller generated energies due to the increase of position resolution.

We utilized the relative difference between the generated and predicted spectra to quantify the systematical error due to energy misclassification. Figure 6(A) shows the muon spectra determined for the test data set (black histogram) and for predicted energies (red histogram). Figure 6(B) shows the corresponding relative differences with black diamonds (errors are within the size of diamonds). This relative difference grows beyond the energy of 6 GeV because the energetic muons suffer fewer deflections and the energy dependency of multiple scattering decreased with the increase of energy. The results shown in Figures 4, 5, and 6 suggest that the actual detector arrangement is applicable to measure the muon spectra up to 6 GeV.

5. SUMMARY

A rotatable muon spectrometer is under development for the measurement of the directional and energy-dependent flux of muons. An MWPC-based particle tracking system has been constructed in the NEWCUT laboratory, Chiba, Japan, at sea level. A neural-network-based analysis method was developed to measure the muons' spectra by classifying their energies on track-by-track

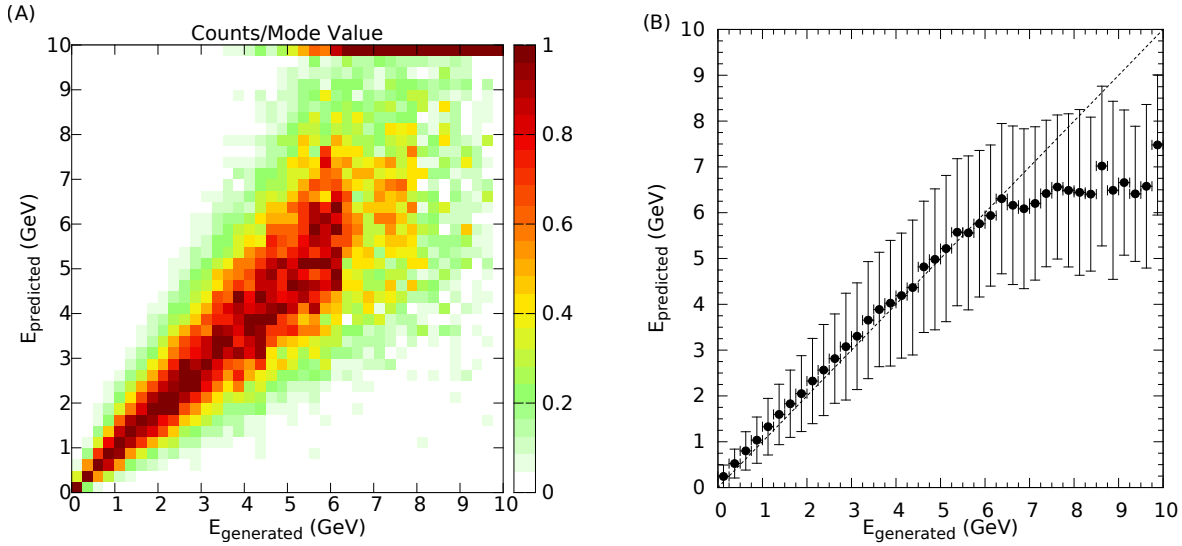

FIGURE 4: (A) The normalized number of muons is shown as a function of generated energy and predicted energy. The number of muons was normalized with the mode of the frequency histogram of predicted energies. (B) The average predicted energies are shown with 1 standard deviation error bars as a function of generated energy. The predicted energies are saturated beyond 6 GeV.

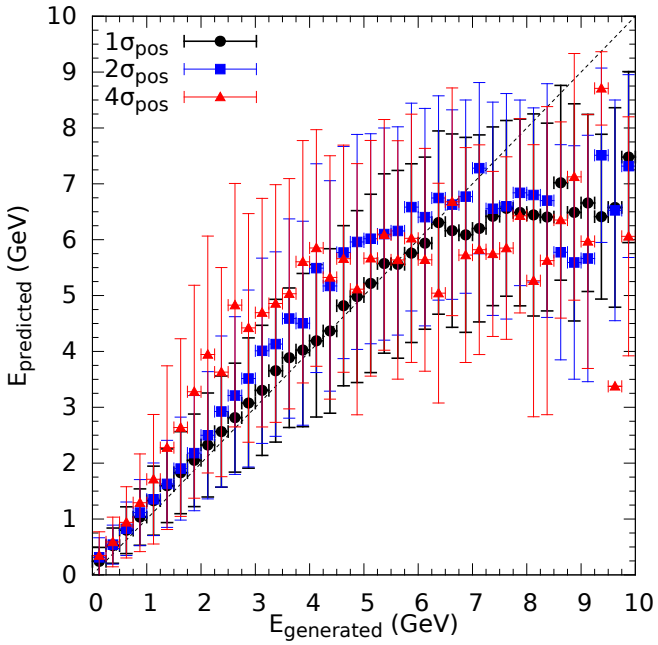

FIGURE 5: The average predicted energies are shown with 1 standard deviation error bars as a function of generated energy for the tracking system with the actual detector segmentation (black circles), two times wider segmentation (blue rectangles), and four times wider segmentation (red triangles), respectively.

basis. The developed model was trained using GEANT4 simulation data. The preliminary results demonstrated that the developed machine learning technique allows measuring the muon spectra up to 6 GeV with the application of a significantly reduced amount of lead plates in the experimental arrangement than in the previous setup [25]. The systematic error originating from the application of the spectra analyzer was also quantified. In the next step, the neural-network-based muon spectra analyzer will be applied to the experimental data.

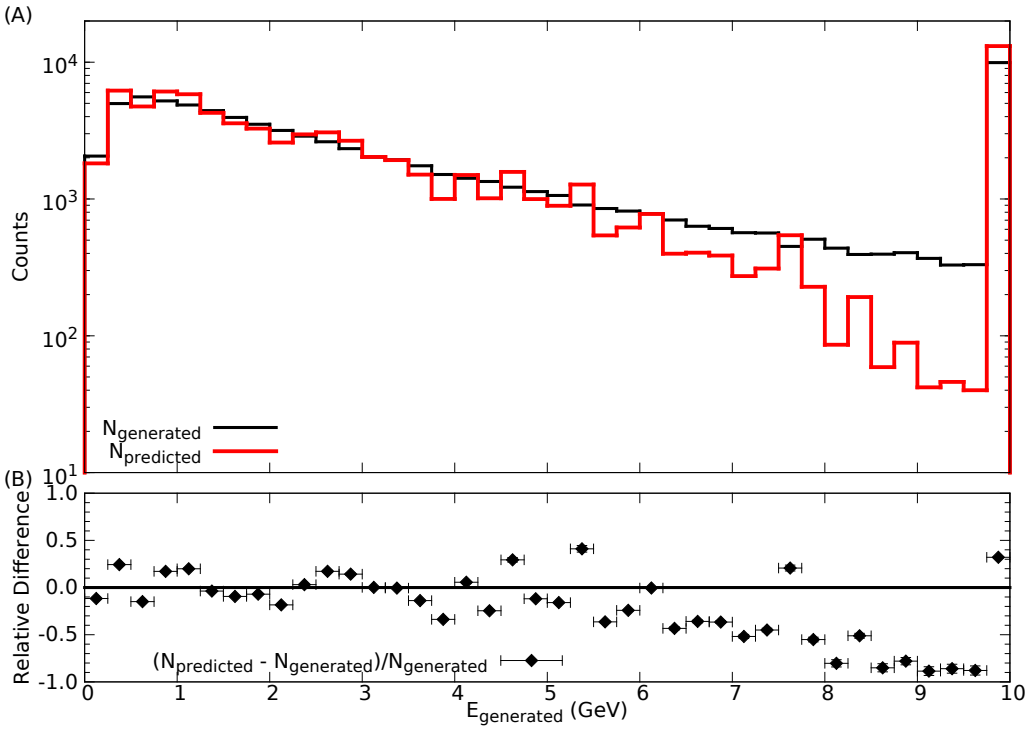

FIGURE 6: (A) The generated (black histogram) and predicted (red histogram) muon spectra. (B) The relative difference between the generated and reconstructed spectra, $(N_{\text{predicted}} - N_{\text{generated}})/N_{\text{generated}}$ (filled diamonds), is shown as a function of energy. The relative difference grows beyond the energy of 6 GeV.

ACKNOWLEDGMENTS

This work is supported by the KAKENHI Project 19H01987, the Joint Usage Research Project (JURP) of the University of Tokyo, Earthquake Research Institute (ERI) under project ID 2020-H-05, the "INTENSE" H2020 MSCA RISE project under Grant Agreement No. 822185, the Hungarian NKFIH research grant under ID OTKA-FK-135349 and TKP-NKTA-10, Wigner Research Centre for Physics of the Eötvös Loránd Research Network, and the Ministry of Education, Culture, Sports, Science and Technology, Japan (MEXT) Integrated Program for the Next Generation Volcano Research. The technical support provided by the members of the REGARD group is gratefully acknowledged. The authors are grateful to an anonymous reviewer for the valuable comments and suggestions that significantly improved the manuscript.

CONFLICTS OF INTEREST

The authors declare that there are no conflicts of interest regarding the publication of this paper.

References

[1] T. Gaisser, Cosmic Rays and Particle Physics. Camb. Uni. Press (1990).
[2] T. Hebbeker and C. Timmermans, A compilation of high energy atmospheric muon data at sea level. Astroparticle Physics **18**, 107–127 *https://doi.org/10.1016/S0927-6505(01)00180-3* (2002).
[3] S. Cecchini and M. Spurio, Atmospheric muons: experimental aspects. *Geosci. Instrum. Method. Data Syst.* **1,** 185–196 *https://doi.org/10.5194/gi-1-185-2012* (2012).
[4] O. C. Allkofer et al., Cosmic ray muon spectra at seal level up to 10 TeV. Nuclear Physics B **259**, 1–18 (1985).
[5] L3 Collaboration, Measurement of the atmospheric muon spectrum from 20 to 3000 GeV. Physics Letters B **598**, 15–32 *https://doi.org/10.1016/j.physletb.2004.08.003* (2004).
[6] L. Bonechi et al., Development of the ADAMO detector: test with cosmic rays at different zenith angles. 29th International Cosmic Ray Conference Pune. **9**, 283–286 (2005).
[7] S. Haino et al., Measurements of primary and atmospheric cosmic-ray spectra with the BESS-TeV spectrometer. Physics Letters B **594**, *https://doi.org/10.1016/j.physletb.2004.05.019* 35–46 (2004).
[8] MACRO Collaboration, Atmospheric neutrino oscillations from upward thoroughgoing muon multiple scattering in MACRO. Physics Letters B **566**, 35–44 *https://doi.org/10.1016/S0370-2693(03)00806-2* (2003).
[9] M. P. De Pascale et al., Absolute Spectrum and Charge Ratio of Cosmic Ray Muons in the Energy Region From 0.2 GeV to 100 GeV at 600 m Above Sea Level. Journal of Geophysical Research **48**, 3501–3507 (1993).

[10] M. Tramontini et al., Middle-Atmosphere Dynamics Observed With a Portable Muon Detector. Earth and Space Science **6** 1865–1876 *https://doi.org/10.1029/2019EA000655* (2019).
[11] K. Kodama et al., Detection and analysis of tau-neutrino interactions in DONUT emulsion target. Nuclear Instruments and Methods in Physics Research A **493** 45–66 (2002).
[12] The ICARUS Collaboration, Measurement of through-going particle momentum by means of multiple scattering with the ICARUS T600 TPC. Eur. Phys. J. C. **48**, 667–676 *https://doi.org/10.1140/epjc/s10052-006-0051-3* (2006).
[13] N. Agafonova et al., Momentum measurement by the multiple Coulomb scattering method in the OPERA lead-emulsion target. New Journal of Physics **14**, 013026 (2012).
[14] The MicroBooNE collaboration, Determination of muon momentum in the MicroBooNE LArTPC using an improved model of multiple Coulomb scattering. Journal of Instrumentation **12**, P10010 *https://doi.org/10.1088/1748-0221/12/10/P10010* (2017).
[15] L. Bonechi, R. D'Alessandro and A. Giammanco, Atmospheric muons as an imaging tool. Reviews in Physics **5** 100038 https://doi.org/10.1016/j.revip.2020.100038 (2020).
[16] G. Bonomi et al., Review Applications of cosmic-ray muons. Progress in Particle and Nuclear Physics **112** 103768 *https://doi.org/10.1016/j.ppnp.2020.103768* (2020).
[17] L. Oláh, H. K. M. Tanaka and D. Varga, Muography: Exploring Earth's Subsurface with Elementary Particles, Geophysical Monograph **270**, ISBN 9781119723028, American Geophysical Union, John Wiley & Sons, Inc. *https://doi.org/10.1002/9781119722748* (2022).
[18] K. N. Borozdin et al., Radiographic imaging with cosmic-ray muons. Nature **422** 277, *https://doi.org/10.1038/422277a* (2003).
[19] R. Nishiyama et al., Monte Carlo simulation for background study of geophysical inspection with cosmic-ray muons. Geophysical Journal International **206**, 1039–1050 *https://doi.org/10.1093/gji/ggw191* (2016).
[20] J. Marteau et al., Implementation of sub-nanosecond time-to-digital convertor in field-programmable gate array: applications to time-of-flight analysis in muon radiography. Meas. Sci. Technol. **25**, 035101 (2014).
[21] G. Gallo et al., Proof-of-Principle of a Cherenkov-Tag Detector Prototype. Sensors **20**, 3437 *https://doi.org/10.3390/s20123437* (2020).
[22] J. Bae and S. Chatzidakis. Fieldable muon spectrometer using multi-layer pressurized gas Cherenkov radiators and its applications. Scientific Reports **12**, 2559 *https://www.nature.com/articles/s41598-022-06510-2* (2022).
[23] H. K. M. Tanaka, T. Kusagaya and H. Shinohara. Radiographic visualization of magma dynamics in an erupting volcano. Nature Communications **5**, 3381 *https://doi.org/10.1038/ncomms4381* (2014).
[24] L. Oláh et al., High-definition and low-noise muography of the Sakurajima volcano with gaseous tracking detectors. Scientific Reports **8**, 3207 *https://doi.org/10.1038/s41598-018-21423-9* (2018).
[25] L. Oláh et al., Improvement of cosmic-ray muography for Earth sciences and civil engineering. Proceedings of Science (ICRC2019) **377** *https://doi.org/10.22323/1.358.0377* (2019).
[26] D. Varga et al., High efficiency gaseous tracking detector for cosmic muon radiography. Advances in High Energy Physics **2016** 1962317 *https://doi.org/10.1155/2016/1962317* (2016).
[27] D. Varga et al., Construction and readout systems for gaseous muography detectors, Journal of Advanced Instrumentation in Science **2022** No. 1. (2022).
[28] S. Agostinelli et al., Geant4 – a simulation toolkit. Nuclear Instruments and Methods in Physics Research A **506** 250–303 *https://doi.org/10.1016/S0168-9002(03)01368-8* (2003).
[29] D. Pagano et al., EcoMug: An Efficient COsmic MUon Generator for cosmic-ray muon applications. Nuclear Instruments and Methods in Physics Research A **1014** 165732 *https://doi.org/10.1016/j.nima.2021.165732* (2021).
[30] A. Géron, Hands-on Machine Learning with Scikit-Learn, Keras & TensorFlow, ISBN 9781492032649, O'Reilly Media (2019).
[31] F. Pedregosa et al., Scikit-learn: Machine Learning in Python. Journal of Machine Learning Research, **12** 2825–2830 *https://www.jmlr.org/papers/v12/pedregosa11a.html* (2011).
[32] Keras, Retrieved from *https://keras.io/* (2020).
[33] Tensorflow, Retrieved from *https://tensorflow.org/* (2020).
[34] Y. LeCun, Y. Bengio and G. Hinton, Deep learning. Nature, **521** 436–444 *https://doi.org/10.1038/nature14539* (2015).
[35] D. P. Kingma and L. J. Ba, Adam: A Method for Stochastic Optimization. International Conference on Learning Representations, *https://arxiv.org/abs/1412.6980v5* (2015).